

Unlocking the Potential of Multimodal Unified Discrete Representation through Training-Free Codebook Optimization and Hierarchical Alignment

Hai Huang^{1†}, Yan Xia^{1†}, Shengpeng Ji¹, Shulei Wang¹, Hanting Wang¹,
Jieming Zhu², Zhenhua Dong², Zhou Zhao^{1*}

¹Zhejiang University, ²Huawei Noah's Ark Lab

Abstract. Recent advances in representation learning have demonstrated the significance of multimodal alignment. The Dual Cross-modal Information Disentanglement (DCID) model, utilizing a unified codebook, shows promising results in achieving fine-grained representation and cross-modal generalization. However, it is still hindered by equal treatment of all channels and neglect of minor event information, resulting in interference from irrelevant channels and limited performance in fine-grained tasks. Thus, in this work, We propose a Training-free Optimization of Codebook (TOC) method to enhance model performance by selecting important channels in the unified space without retraining. Additionally, we introduce the Hierarchical Dual Cross-modal Information Disentanglement (H-DCID) approach to extend information separation and alignment to two levels, capturing more cross-modal details. The experiment results demonstrate significant improvements across various downstream tasks, with TOC contributing to an average improvement of 1.70% for DCID on four tasks, and H-DCID surpassing DCID by an average of 3.64%. The combination of TOC and H-DCID further enhances performance, exceeding DCID by 4.43%. These findings highlight the effectiveness of our methods in facilitating robust and nuanced cross-modal learning, opening avenues for future enhancements. The source code and pre-trained models can be accessed at https://github.com/haihuangcode/TOC_H-DCID.

Keywords: Unified Discret Representation · Training-free Optimization · MultiModal Alignment

1 Introduction

Humans' capacity to integrate multimodal information, such as text, audio, and visual, has inspired research on extracting unified information from multimodal data [10, 16, 17, 23]. Researchers aim to develop models that learn unified representations across modalities, using techniques like contrastive learning to map

* Corresponding Author † Equal Contribution

semantically similar multimodal data closer in the embedding space [14, 21, 32], achieving notable results in downstream tasks like zero-shot and cross-modal retrieval. However, the unbounded nature of the continuous embedding space poses challenges in interpretability. To address this, recent works have explored constructing discrete embedding spaces with prototypes or codebooks, enhancing cross-modal learning and model interpretability [8, 11, 13, 36]. Nevertheless, these methods might be less effective in complex scenarios, such as audio-visual localization tasks in misaligned situations, due to their assumption of complete alignment of modal information.

To address the aforementioned challenges, Xia *et al.* [31] proposed Uni-code. Their method utilizes a codebook as the discrete embedding space for a unified representation of multimodal data and introduces the Dual Cross-modal Information Disentanglement (DCID) module. The core concept of this approach is to distinguish and refine the shared semantic content within cross-modal data while eliminating the redundant information specific to each modality. This design philosophy enables the model to learn a more refined and universal cross-modal representation, capable of extracting common semantics even in the absence of perfect alignment between modalities. Consequently, this approach enhances the model’s performance in more complex tasks.

While Uni-code [31] has demonstrated incredible achievements in multimodal unified representation, there are limitations in terms of the efficiency of embedding space utilization and the granularity of alignment. **1)** According to previous work [3, 30], the significance of features varies across different channels, and the selection of appropriate channels can accelerate inference speed and enhance model performance. However, Uni-code and preceding efforts [11, 13, 36] overlook this issue due to the inherent constraints of the codebook and the quantization method based on Euclidean distance. This approach treats all channels equally without considering the importance of individual channels, resulting in interference from irrelevant channel information. **2)** During the pre-training process, models primarily focus on aligning the common major information, emphasizing the alignment of shared events across modalities. However, this approach may neglect critical event information unique to a specific modality, thereby constraining the model’s performance in fine-grained tasks.

Inspired by the concept of feature importance [3, 30, 33, 40] and the training-free adapter in tip-adapter [35], we introduce the Training-free Optimization of Codebook (TOC) mechanism to address limitation **1**. TOC optimizes the codebook through calculations without requiring additional training parameters, thereby enhancing the ability to compute and select features within the codebook of the Uni-code pre-trained model in downstream tasks. This approach achieves a training-free effect improvement, reducing additional training costs and decreasing the training parameter requirements for downstream tasks.

As illustrated in Fig. 1(b), TOC selects specific channels from quantized features for downstream tasks and feeds them into the decoder. This selection process is completed after pre-training and does not require recalculation for

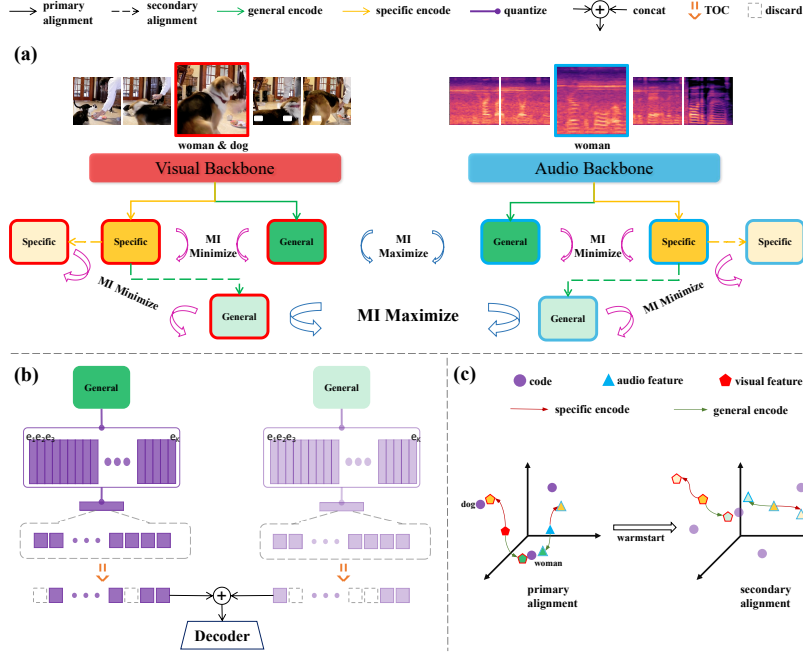


Fig. 1: (a)H-DCID encoder architecture (b) The process of training or testing a downstream task using H-DCID+TOC for a specific modality, where the Decoder’s parameters are updated during training and frozen during testing, while the parameters of other modules remain frozen throughout. (c)Illustration of H-DCID at the third second in (a): primary alignment initiated at pre-training onset, secondary alignment activated after specified epochs

different downstream tasks. This approach significantly enhances the efficiency and effectiveness of downstream task execution.

As for limitation 2, we design a new framework: Hierarchical Dual Cross-modal Information Disentanglement (H-DCID) illustrated in Fig. 1(a). H-DCID retains the advantages of DCID [31] in achieving unified multimodal expression while significantly enhancing the model’s flexibility and precision in processing fine-grained information through a hierarchical alignment mechanism.

As illustrated in Fig. 1(c), the visual modality encompasses information about a dog and a woman, while the audio modality encompasses only the women. In the traditional DCID framework, information about the dog is disregarded as modality-specific, resulting in the exclusion of relevant visual events. This poses a challenge for audio-to-visual cross-modal generalization tasks, as the audio label lacks information about the dog. To address this, we propose a further alignment step, focusing on this specific information. We introduce a secondary alignment process to extract and align this information effectively. To ensure the robustness of this secondary alignment, we employ a warm-start technique,

initiating the secondary alignment training only after the primary alignment is completed.

The main contributions of this work are summarized as follows:

- We propose the **TOC**, a novel approach that precisely identifies the importance of channels through calculations without the need for additional training. To the best of our knowledge, this is the first attempt at training-free optimization of the codebook, and we have demonstrated its universality and transferability to other scenarios.
- We introduce **H-DCID**, which employs a hierarchical alignment strategy to extract primary and secondary alignment events in multimodality. This approach significantly improves the model’s ability to understand details and has shown considerable performance enhancements in downstream tasks with higher granularity requirements.
- Our method significantly outperformed the previous best model, DCID, across various tasks in the cross-modal generalization setup, showcasing its effectiveness in multimodal learning. Specifically, TOC, H-DCID, and their combination outperformed DCID [31] by 1.70%, 3.64%, and 4.43% respectively, on four downstream tasks. Additionally, we explored the impact of different quantization methods on the codebook, providing valuable insights for future research in this area.

2 Related Work

Multi-Modal Unified Representation: In recent years, significant efforts have been devoted to multi-modal unified representations, including approaches that implicitly align different modalities into the same latent space [1, 20, 22] and strategies that train modality-general encoders to extract information across modalities [5, 29]. Techniques such as cross-modal knowledge distillation facilitate knowledge transfer between modalities [19, 22], while unified expressions are often formed using codebook or prototype [8, 11, 13, 36]. Duan *et al.* [8] employs Optimal Transport to map feature vectors from different modalities to prototypes. Zhao *et al.* [36] utilize self-cross-reconstruction to enhance mutual information. Liu *et al.* [11] employs a similar scheme to align videos with speech/text, but they assume perfect alignment between modalities. Xia *et al.* [31] addresses the challenge of non-perfectly aligned multimodal sequences by mapping them into a common discrete semantic space through rational information decoupling.

Training Free Optimization: Recent works have explored diverse approaches to enhance model performance without additional training. The Training-Free CLIP-Adapter (Tip-Adapter) [35] and the Adaptive Prior rEfinement (APE) method [40] leverage non-parametric and refinement techniques, respectively, to improve few-shot classification capabilities of the CLIP model. In diffusion models, a novel training-free method [4] optimizes time steps and model architecture for efficient image generation, while the FuseDream pipeline [12] employs a CLIP+GAN approach for robust text-to-image generation. Beyond CLIP-based

models, the TEEN method [28] offers a training-free approach for few-shot class-incremental learning, efficiently recognizing new classes without training costs. Building on these advancements, this paper introduces TOC, which, to the best of our knowledge, represents the first exploration of training-free optimization within the context of multimodal unified discrete representation. This work further extends the scope of training-free approaches in the field.

3 Background

Dual Cross-modal Information Disentanglement (DCID) [31] is a framework designed to align primary common events across modalities by disentangling and refining shared semantic content within cross-modal data. It employs modality-specific encoders Ψ^m to extract modality-specific features $\bar{\mathbf{z}}_i^m$ and modality-general encoders Φ^m to extract modality-general features \mathbf{z}_i^m from modalities $m \in \{a, b, c\}$. The framework optimizes mutual information (MI) between these features to minimize redundancy and enhance semantic alignment.

Mutual Information Minimization: DCID utilizes the CLUB [6] method to minimize the MI between modality-general and modality-specific information within each modality:

$$\hat{I}_{\text{vCLUB}} = \frac{1}{N} \sum_{i=1}^N \left[\log q_{\theta}(\bar{\mathbf{z}}_i^m | \mathbf{z}_i^m) - \frac{1}{N} \sum_{j=1}^N \log q_{\theta}(\bar{\mathbf{z}}_j^m | \mathbf{z}_i^m) \right], \quad (1)$$

where q_{θ} is the variational approximation of the ground-truth posterior, N is the number of samples, and m denotes the modality.

Mutual Information Maximization: To maximize MI across different modalities, DCID employs Cross-Modal CPC [18], predicting future samples in one modality using context representations from another modality. The objective is formulated as:

$$L_{\text{cpc}} = -\frac{1}{R} \sum_{r=1}^R \log \left[\frac{\exp(\mathbf{z}_{t+r}^n W_r^m \mathbf{c}_t^m)}{\sum_{\mathbf{z}_j \in Z_n} \exp(\mathbf{z}_j^n W_r^m \mathbf{c}_t^m)} \right], \quad (2)$$

where W_r^m is a learnable weight matrix, \mathbf{c}_t^m is the context representation, R is the prediction horizon, t is the time step, and Z_n is a set of negative samples.

Cross Modal Generalization (CMG) is a task introduced by Xia *et al.* [31] that evaluates the model’s ability to map diverse modalities, such as text, audio, and video, into a unified discrete latent space. The model’s ability for cross-modal zero-shot knowledge transfer is evaluated through a setup where training is conducted on modality $m1$ and testing is performed on modality $m2$.

During training, the model learns a representation for inputs from one modality using the encoder Φ^{m1} and the downstream decoder \mathbf{D} :

$$\mathbf{E}(\mathbf{D}(VQ(\Phi^{m1}(\mathbf{x}_i^{m1}))), \mathbf{y}_i^{m1}), \quad (3)$$

where \mathbf{x}_i^{m1} is the input, \mathbf{y}_i^{m1} is the label, and \mathbf{E} is the evaluation function. During testing, the model is evaluated on a different modality $m2$, demonstrating its ability to generalize:

$$\mathbf{E}(\mathbf{D}(VQ(\Phi^{m2}(\mathbf{x}_i^{m2}))), \mathbf{y}_i^{m2}). \quad (4)$$

Here, $m1, m2 \in a, b, c$ and $m1 \neq m2$. The parameters of both Φ^{m1} and Φ^{m2} are parameters frozen during training and testing, while only the parameters of \mathbf{D} are updated during training.

4 Method

In this section, we introduce the proposed Training-free Optimization Codebook (TOC) and Hierarchical Dual Cross-modal Information Disentanglement (H-DCID) to significantly explore the potential of DCID [31] in multimodal generalization. In Section 4.1, we introduce the two internal code metrics that constitute TOC. In Section 4.2, we introduce the design rationale of H-DCID and provide a detailed exposition of their differences.

4.1 Training-free Optimization Codebook

Discrete unified representation spaces commonly employ a codebook structure, where modalities are updated based on the Euclidean distance between their features and the codebook codes. This channel-equal-weighted update strategy does not consider the varying importance of channels, leading to redundancy in the final discrete space. Therefore, we propose two metrics, Inter-Code Similarity and Inter-Code Variance, to refine the information in the unified space. It is worth noting that, unlike the APE [40], which refines features using downstream few-shot information to calculate the most significant feature channels, TOC targets the pre-trained codebook and can complete calculations without downstream information. Furthermore, TOC addresses more complex downstream tasks, whereas APE is limited to image classification.

Inter-code Similarity: This metric aims to enhance the distinctiveness of codes by extracting feature channels that minimize code similarity. We represent the unified representation codebook of modalities as $\mathbf{e} \in \mathbb{R}^{L \times D}$, where L, D denote the size of the discrete latent space and hidden dimension, respectively.

Assuming the existence of a classification dataset with C categories, acquiring its complete data enables the calculation of the average similarity, denoted as S . In an open-world setting, we may assume that the prior probabilities of all categories are equal, denoted as $\frac{1}{C}$. We adopt cosine similarity, $\delta(\cdot, \cdot)$, as the chosen metric:

$$S = \frac{1}{C^2} \sum_{i=1}^C \sum_{\substack{j=1 \\ j \neq i}}^C \frac{1}{N^i N^j} \sum_{m=1}^{N^i} \sum_{n=1}^{N^j} \delta(\mathbf{x}^{i,m}, \mathbf{x}^{j,n}), \quad (5)$$

where $\mathbf{x}^{i,m}$ and $\mathbf{x}^{j,n}$ denote the input features for the m -th and n -th samples of categories i and j , respectively. N^i and N^j represent their respective total number of training samples.

Each code in the codebook, $\mathbf{e}^i \in \mathbb{R}^D, i \in [0, L)$, can be considered as a distinct semantic cluster center, representing a category. Therefore, we can simplify the average similarity calculation by considering each code as representing one category:

$$S = \frac{1}{L^2} \sum_{i=1}^L \sum_{\substack{j=1 \\ j \neq i}}^L \delta(\mathbf{e}^i, \mathbf{e}^j), \quad (6)$$

Our goal is to select Q channels out of D to enhance the distinctiveness of the codes. We introduce a binary flag $\mathbf{F} \in \{0, 1\}^D$, where $F_k = 1$ ($k = 1, \dots, D$) indicates that the k^{th} channel \mathbf{e}_k^i is selected, and $\mathbf{F}\mathbf{F}^\top = Q$. Our objective now becomes finding the optimal \mathbf{F} to minimize the Inter-Code Similarity:

$$\min_{\mathbf{F}} S = \frac{1}{L^2} \sum_{i=1}^L \sum_{\substack{j=1 \\ j \neq i}}^L \delta(\mathbf{e}^i \odot \mathbf{F}, \mathbf{e}^j \odot \mathbf{F}), \quad (7)$$

where \odot denotes element-wise multiplication.

We further suppose the Codebook has been L2-normalized, meaning that each code vector $\mathbf{e}^i \in \mathbb{R}^D$ has a unit length. Under this assumption, the cosine similarity between two code vectors \mathbf{e}^i and \mathbf{e}^j can be simplified as their dot product:

$$\delta(\mathbf{e}^i, \mathbf{e}^j) = \mathbf{e}^i \cdot \mathbf{e}^j, \quad (8)$$

where \cdot denotes the dot product of two vectors. Then we can simplify the cosine similarity as

$$S = \sum_{k=d_1}^{d_Q} S_k = \sum_{k=d_1}^{d_Q} \left(\frac{1}{L^2} \sum_{i=1}^L \sum_{\substack{j=1 \\ j \neq i}}^L \mathbf{e}_k^i \cdot \mathbf{e}_k^j \right), \quad (9)$$

where $k = \{d_1, d_2, \dots, d_Q\}$ denotes the indices of selected feature channels with $F_k = 1$, and $S_k = \frac{1}{L^2} \sum_{i=1}^L \sum_{\substack{j=1 \\ j \neq i}}^L \mathbf{e}_k^i \cdot \mathbf{e}_k^j$ represents the average inter-class similarity of the k^{th} channel. Through straightforward derivation, we observe that solving the optimization problem is equivalent to selecting Q elements with the smallest average similarity.

Inter-code Variance: Our objective is to minimize redundancy by eliminating feature channels with low variance across codewords, as such channels contribute limited discriminative information. In this framework, codewords are regarded as distinct semantic cluster centers. The variance for the k^{th} feature channel is formulated as:

$$V_k = \frac{1}{L} \sum_{i=1}^L (\mathbf{e}_k^i - \bar{\mathbf{e}}_k)^2, \quad (10)$$

where $\bar{\mathbf{e}}_k = \frac{1}{L} \sum_{i=1}^L \mathbf{e}_k^i$ represents the mean of the k^{th} channel across all code-words. Analogous to Inter-code Similarity, we select the Q channels exhibiting the highest variance to augment discriminative power.

To amalgamate the criteria of similarity and variance, a balance factor λ is introduced to compute the final metric for each feature channel:

$$J_k = \lambda S_k - (1 - \lambda) V_k, \quad (11)$$

where $k = 1, \dots, D$. The channels corresponding to the top- Q smallest values of J_k are chosen as the refined features, maximizing inter-class divergence and discrimination.

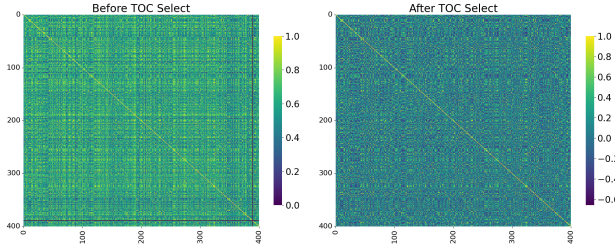


Fig. 2: The left image illustrates the heatmap obtained from direct cosine similarity calculations between the codes, while the right image displays the heatmap obtained from cosine similarity calculations between the codes after selecting the 128 most important dimensions through TOC.

We conducted an evaluation of TOC on the open-source pre-trained model of DCID [31]. The unified discrete representation space of this model is a Codebook consisting of 400 vectors, each with 256 dimensions. As depicted in Fig. 2, the distinctiveness of the codes with the 128-dimensional features obtained after TOC computation is notably enhanced.

4.2 Hierarchical Dual Cross-modal Information Disentanglement

H-DCID extends DCID [31] by introducing a hierarchical structure to capture both primary and secondary cross-modal events. The architecture consists of two layers:

First Layer: Similar to DCID, the first layer of H-DCID aligns primary common events across modalities. It utilizes a set of modality-specific encoders $\{\Psi_1^m\}_{m=a,b,c}$ and modality-general encoders $\{\Phi_1^m\}_{m=a,b,c}$ to extract features $\{\bar{\mathbf{z}}_1^m\}_{m=a,b,c}$ and $\{\mathbf{z}_1^m\}_{m=a,b,c}$, respectively, and align $\{\mathbf{z}_1^m\}_{m=a,b,c}$ in a shared latent space. The vector quantization process maps these features to discrete codes in the codebook $\mathbf{e}_1 \in \mathbb{R}^{L \times D}$.

Second Layer: The second layer targets the alignment of secondary events that are unique to individual modalities. It operates with the modality-specific features $\{\bar{\mathbf{z}}_1^m\}_{m=a,b,c}$ extracted in the first layer as input and employs a separate set of encoders $\{\Psi_2^m\}_{m=a,b,c}$ and $\{\Phi_2^m\}_{m=a,b,c}$ to further refine the alignment.

This layer has another codebook $\mathbf{e}_2 \in \mathbb{R}^{L \times D}$ as the unified space for quantizing the modality-general result after alignment. The encoder architecture is shown in Fig. 1(a).

Mutual Information Minimization: To disentangle the shared and modality-specific information, H-DCID minimizes the mutual information between the modality-general and modality-specific features. The objective function for this process is denoted as L_{MI} , which is formulated based on the CLUB [6] method:

$$\hat{I}_{v\text{CLUB}} = \frac{1}{N} \frac{1}{K} \sum_{i=1}^N \sum_{k=1}^K \left[\frac{1}{T} \sum_{t=1}^T \log q_{\theta}(\bar{\mathbf{z}}_{i,k}^m | \mathbf{z}_{i,k}^m) - \frac{1}{N} \frac{1}{T} \sum_{j=1}^N \sum_{t=1}^T \log q_{\theta}(\bar{\mathbf{z}}_{j,k}^m | \mathbf{z}_{i,k}^m) \right],$$

$$m \in \{a, b, c\}, k \in \{1, 2\}.$$
(12)

Mutual Information Maximization: Conversely, H-DCID maximizes the mutual information across modality-general features from different modalities to ensure that the shared latent space captures the common semantic content. This is achieved using a cross-modal contrastive predictive coding approach, denoted as L_{cpc} :

$$L_{\text{cpc}}^{m2n} = -\frac{1}{R} \frac{1}{K} \sum_{r=1}^R \sum_{k=1}^K \log \left[\frac{\exp(\mathbf{z}_{t+r,k}^n W_{r,k}^m \mathbf{c}_{t,k}^m)}{\sum_{\mathbf{z}_j \in Z_n} \exp(\mathbf{z}_{j,k}^n W_{r,k}^m \mathbf{c}_{t,k}^m)} \right], m, n \in \{a, b, c\}, k \in \{1, 2\}.$$
(13)

Where K represents the two-layer alignment, and the overall objective of H-DCID is a combination of these loss functions across both layers:

$$L = L_{\text{recon}} + L_{\text{commit}} + L_{\text{cpc}} + L_{\text{cmcm}} + L_{\text{MI}}, \quad (14)$$

where L_{recon} is the reconstruction loss, L_{commit} is the commitment loss, L_{cpc} is the Contrastive Predictive Coding loss [18], L_{cmcm} is the cross-modal alignment loss, and L_{MI} is $\hat{I}_{v\text{CLUB}}$. The appendix provides detailed derivations or explanations for all formulas and losses.

The hierarchical structure of H-DCID, with its two-layer approach, provides a more comprehensive representation of multimodal data compared to DCID [31]. This enhanced representation enables H-DCID to perform better in downstream tasks that require a fine-grained semantic understanding, by capturing both primary and secondary cross-modal events.

5 Experiment

5.1 Datasets and Tasks

Pre-train: The pretraining dataset uses the VGGsound-AVEL [37, 39] with prompts provided by Xia *et al.* [31], divided into three sizes: 24K, 40K, 81K.

Downstream: The pre-trained models will be evaluated on several downstream tasks using different datasets. **Cross-modal event classification on AVE dataset:** [27] training on one modality (*e.g.* video) and evaluating on another (*e.g.* audio). **Cross-modal event localization on AVVP dataset:** [26] localizing events in one modality and transferring to the other. **Cross-dataset localization/classification:** training on classification in AVE and evaluating localization in AVVP, transferring across datasets. Cross-modal classification between UCF-101 [25] visual clips and VGGSound-AVEL audio clips. **Cross-modal video segmentation on AVSBench-S4 dataset:** [38] segmenting video based on an audio or text query.

Table 1: Comparison of DCID and H-DCID performance on four downstream tasks and the impact of TOC(pre-trained on audio-visual-text modalities)

DCID [31]	H-DCID-Layer	TOC	VGGsounds-AVEL 40K									
			AVE		AVVP		AVE→AVVP		UCF(v)↔VGG(a)		Avg.	
			V→A	A→V	V→A	A→V	V→A	A→V	V→A	A→V		
✓	-	-	54.1	55.0	63.4	71.0	53.0	52.4	67.1	60.6	59.58	
✓	-	✓	54.5	55.0	66.1	74.7	56.5	53.6	68.1	61.7	61.28	
-	1	-	49.4	53.5	60.4	77.2	53.4	52.9	70.6	59.5	59.61	
-	2	-	49.0	54.4	74.1	88.0	57.7	53.9	69.5	59.1	63.22	
-	2	✓	49.0	54.9	76.0	91.0	54.4	55.9	70.7	60.2	64.01	

Table 2: Impact of different quantization methods on DCID and H-DCID: grey rows indicate results for the training modality of the previous row and their averages exclude AVE2AVVP, while averages for the remaining rows include eight results(pre-trained on audio-visual-text modalities)

FSQ	RVQ-Layer	DCID [31]	H-DCID	VGGsounds-AVEL 40K									
				AVE		AVVP		AVE→AVVP		UCF(v)↔VGG(a)		Avg.	
				V→A	A→V	V→A	A→V	V→A	A→V	V→A	A→V		
-	1	✓	-	54.1	55.0	63.4	71.0	53.0	52.4	67.1	60.6	59.58	
Evaluation results of the labeled modality				64.8	65.8	71.0	72.9	-	-	80.0	85.4	73.32	
✓	1	✓	-	45.2	50.4	48.1	54.9	51.4	44.0	67.1	60.6	52.71	
Evaluation results of the labeled modality				76.5	78.2	65.8	72.1	-	-	98.5	92.2	80.55	
-	4	✓	-	48.5	55.5	58.7	68.6	56.3	54.7	69.4	64.3	59.50	
Evaluation results of the labeled modality				69.9	70.3	75.1	75.6	-	-	88.0	90.8	78.28	
-	1	-	✓	49.0	54.4	74.1	88.0	57.7	53.9	69.5	59.1	63.22	
Evaluation results of the labeled modality				63.8	65.0	71.1	73.9	-	-	80.7	85.2	73.28	
-	2	-	✓	44.9	52.7	65.6	78.6	54.6	53.6	72.7	67.3	61.25	
-	3	-	✓	41.8	52.7	65.3	75.0	53.5	53.6	69.3	60.0	58.90	
-	4	-	✓	44.4	52.3	67.9	82.8	50.9	51.8	71.1	68.1	61.16	

5.2 Implementation Details

We employ DCID [31] as the baseline and compare its performance with recent works on unified representations, including S-Mit [17], MST [34], CODIS [8], TURN [36], and CMCM [11]. These methods are implemented on our tasks, and their performance is evaluated on two downstream tasks. For the AVE [27], VGGSound-AVEL [37,39], and UCF101 [25] datasets, precision (%) is used as the

metric. Accuracy (%) is employed for evaluating performance on the AVVP [26] datasets. The F1-score (%) is utilized for assessing the AVE to AVVP generalization task, while mIoU and F-score (as defined in AVS [38]) are used for the AVS-S4 dataset.

The losses of H-DCID are not suitable for full backpropagation initially. If subsequent layer losses participate in backpropagation before sufficient disentanglement is achieved by previous layers, this can lead to failure in aligning modality-general semantics from coarse to fine granularity across layers. We use the warm-start technique, applying only preceding layer losses for the first few epochs until adequate disentanglement is reached. Only then are losses from subsequent DCID [31] layers introduced into the backpropagation.

All results presented in Tabs. 1 to 5 were obtained with the codebook size set to 400. The ablation study on codebook size is discussed in Fig. 5. The backbone models used to extract features for video, audio, and text modalities are VGG19 [24], VGGish, and BERT [7], respectively.

Table 3: Comparison with state-of-the-art methods on two downstream tasks(pre-trained on audio-visual modalities)

Method	VGGsounds-AVEL 24K				VGGsounds-AVEL 40K				VGGsounds-AVEL 81K				Avg.
	AVE		AVVP		AVE		AVVP		AVE		AVVP		
	V→A	A→V	V→A	A→V	V→A	A→V	V→A	A→V	V→A	A→V	V→A	A→V	
S-Mit [17]	12.7	16.9	17.2	22.8	14.4	15.9	19.0	22.3	13.4	17.0	20.9	22.8	17.94
MST [34]	13.3	19.0	25.7	29.1	19.5	23.1	22.7	24.5	18.6	20.5	19.1	24.8	21.66
CODIS [8]	18.5	22.0	29.4	33.7	20.8	26.4	35.1	37.9	28.5	30.2	34.0	37.8	29.53
TURN [36]	17.7	21.0	29.4	32.4	19.1	24.3	36.9	39.3	27.6	31.4	33.8	38.1	29.25
CMCM [11]	28.9	35.9	42.6	50.4	32.7	36.8	41.9	45.1	31.1	34.0	39.3	44.8	38.63
DCID+S-Mit	28.1	32.3	45.9	49.2	32.2	34.0	47.8	53.0	34.8	37.6	51.9	53.5	41.69
DCID+MST	31.2	35.0	50.7	52.1	34.9	37.8	54.4	59.1	33.5	35.4	57.1	59.2	45.03
DCID+TURN	29.4	35.3	53.4	56.0	29.7	36.9	55.2	58.2	31.9	36.8	56.2	60.9	44.99
DCID+CODIS	33.4	36.0	53.8	60.2	36.7	41.0	52.6	62.0	35.9	40.1	54.3	59.0	47.08
DCID+CMCM	34.1	38.8	57.6	60.8	36.4	42.9	58.7	62.8	38.8	41.4	57.5	60.5	49.19
H-DCID+S-Mit	25.9	30.4	51.0	57.7	30.7	33.4	52.8	61.2	33.6	36.2	55.3	60.2	44.03
H-DCID+MST	27.9	34.3	56.9	60.7	31.9	36.1	59.5	65.9	31.3	34.2	59.3	63.1	46.76
H-DCID+TURN	26.6	33.9	58.4	64.6	27.7	35.9	60.4	66.9	27.0	35.9	60.5	65.2	46.92
H-DCID+CODIS	31.0	34.8	59.8	67.6	35.4	40.2	56.3	69.7	34.6	40.3	55.6	67.4	49.39
H-DCID+CMCM	32.1	37.3	63.9	68.7	35.3	42.5	63.9	70.8	35.0	42.2	63.5	69.5	52.06
DCID [31] full modal	44.0	49.7	61.9	65.7	47.7	52.3	64.0	65.6	41.2	45.6	60.5	61.7	54.99
H-DCID full modal	41.9	47.9	66.7	72.9	44.8	51.1	69.3	76.5	40.2	44.7	65.2	71.5	57.73

5.3 Performance Analysis

TOC: As shown in Tab. 1, a comparison between the first and second rows reveals that TOC improves DCID’s performance in seven out of eight results, excluding the AVE [27] task in the a2v direction. Notably, six results in the last three downstream tasks show at least a 1.0% increase, with an average improvement of 1.7%. Comparing the fourth and fifth rows, H-DCID with TOC shows a slight decrease only in the a2v direction from AVE to AVVP, while the other results remain stable or improve, with an average increase of 0.79%. These findings demonstrate the effectiveness of TOC in optimizing the unified discrete representation for various downstream scenarios.

H-DCID: We compare our model with leading methods on two downstream tasks: cross-modal event classification and localization. All models are pre-trained using audio-visual modalities on three different dataset sizes. As shown in Tab. 3, these state-of-the-art methods face challenges in unconstrained audio-visual alignment. Adding DCID [31] or H-DCID improves their performance on both tasks. However, DCID and H-DCID differ in their improvement directions. H-DCID shows a tradeoff between semantic alignment and task performance compared to DCID. In the classification task, which relies more on high-level semantics, H-DCID has a slight decrease in accuracy compared to DCID. In the event localization task, which requires finer-grained alignment, H-DCID shows more significant improvement.

Considering the specificity of the AVVP [26] localization task, where audio and video events are not always identical, the notable improvement in AVVP indicates that H-DCID’s secondary alignment effectively extracts minor events. Unfortunately, this also introduces noise from non-primary aligned events in the AVE classification task, leading to a slight decrease in results. However, the decrease in AVE [27] is much smaller compared to the improvement in AVVP.

Comparing the third and fourth rows of Tab. 1 further supports this observation. When both alignment layers are utilized, there is a slight decrease in H-DCID’s performance for AVE [27] and UCF2VGG, which are tasks with coarse-grained classification.

Tab. 3 also indicates that the volume of pre-training data impacts downstream task performance. Increasing data from 24K to 40K improves performance, but further expansion to 81K does not yield significant gains and may even slightly reduce performance. This suggests that an optimal amount of data is needed for effective pre-training. Beyond a certain point, additional data may not provide value and could introduce noise. Thus, the scale of pre-training data should be carefully balanced with model capacity and alignment objectives.

Quantization Method We evaluated the impact of Residual Vector Quantization (RVQ) [2] and Finite Scalar Quantization (FSQ) [15] on four downstream tasks, as detailed in Tab. 2. When RVQ-Layer is set to 1, it is equivalent to vector quantization. Observing rows 3 to 6, the primary advantage of RVQ and FSQ is the improvement in average performance on labeled modalities, which increased from 71.32% to 78.28% and 80.55%, respectively. This substantial improvement indicates that their precise quantization enhances reconstruction by reducing training bias through more accurate codebook mapping. However, cross-modal generalization decreased, suggesting that neither RVQ nor FSQ alone can further extract modality-general representations.

FSQ performs poorly on cross-modal tasks because its codebook space is fixed and does not update during the experiment, thus failing to enhance the ability of unified representation. RVQ maintains better cross-modal generalization capability, related to its update strategy similar to Vector Quantization (VQ), but its cross-modal generalization is still inferior to VQ.

As shown in Fig. 3, H-DCID resembles RVQ in its formal structure. If we analogize the modal-specific result and the modal-general result to the residual

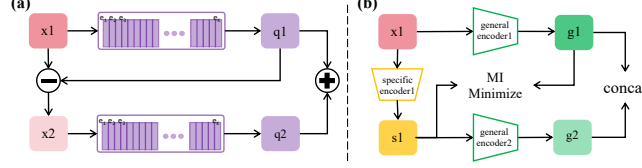


Fig. 3: (a) Two-layer RVQ-DCID (b) Simplified diagram of H-DCID

result after quantization and the quantized value, respectively, H-DCID can be seen as equivalent to a two-layer RVQ-DCID. However, RVQ underperforms compared to H-DCID because each quantization step in RVQ does not encapsulate independent semantics; it requires summation to derive the true semantic meaning. In contrast, H-DCID generates independent semantics through its encoding process, meaning that each layer of the modal-general result possesses its distinct semantics. Consequently, H-DCID enriches the original DCID framework with more comprehensive information.

Results on AVS-S4: A2T refers to the semantic segmentation of videos using audio for training and text for testing, with T2A being the opposite. As shown in Tab. 4 and Fig. 4, we evaluated model alignment between audio and text modalities on a semantic segmentation task that segments video using audio [38]. Both DCID and H-DCID achieved performance close to the original paper on this task, demonstrating the effectiveness of our pre-trained model in transferring semantic segmentation ability between audio and text modalities, thereby expanding the original dataset to enable text-based segmentation.

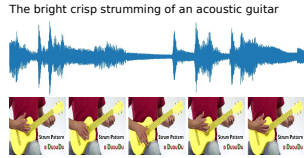


Fig. 4: Result demonstration semantic segmentation on AVS

Methods	A2T		T2A	
	mIoU	F-score	mIoU	F-score
DCID	78.0	87.1	77.7	86.7
H-DCID	78.1	87.0	77.8	86.9
SST [9] (A2A)	60.3	80.1	-	-
AVS [38] (A2A)	78.7	87.9	-	-

Table 4: Performance on AVS-S4 datasets (pre-trained on audio-visual-text modalities)

Table 5: Ablation studies on the impact of TOC on DCID(pre-trained on audio-visual-text modalities)

Inter-code Similarity	Inter-code Variance	VGGsounds-AVEL 40K									
		AVE		AVVP		AVE→AVVP		UCF(v)↔VGG(a)		Avg.	
		V→A	A→V	V→A	A→V	V→A	A→V	V→A	A→V		
-	-	54.1	55.0	63.4	71.0	53.0	52.4	67.1	60.6	59.58	
✓	-	53.8	55.0	62.0	73.0	56.6	53.6	67.4	61.8	60.40	
-	✓	53.8	54.7	60.2	67.3	54.0	55.3	67.2	61.9	59.30	
✓	✓	54.5	55.0	66.1	74.7	56.5	53.6	68.1	61.7	61.28	

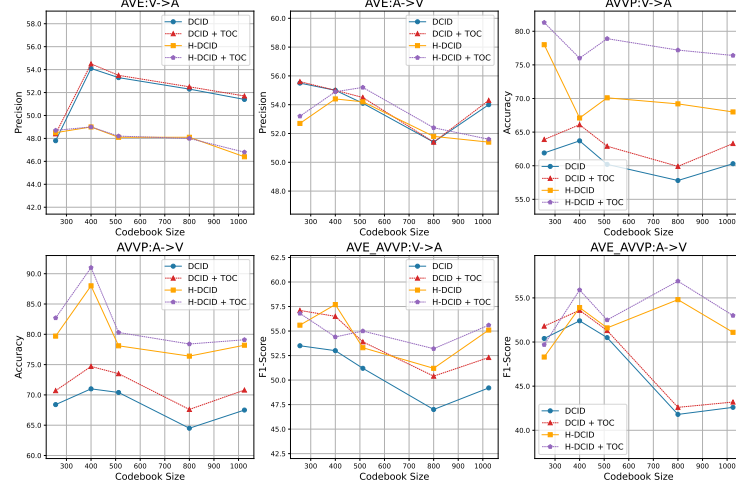


Fig. 5: Impact of codebook size on performance in two downstream tasks for DCID and H-DCID models

5.4 Ablation Study

TOC and H-DCID: As shown in Tab. 5, optimizing channels solely based on Inter-code Similarity can enhance the model’s average performance by 0.82%. In contrast, using channels optimized solely based on Inter-code Variance leads to a decrease in model performance. However, when used together with Inter-code Similarity, Inter-code Variance can further improve the model’s performance, with an average increase of 1.7%. This suggests that a combined approach, leveraging both similarity and variance optimization, is more effective in enhancing the model’s performance. The structure of H-DCID is similar to that of DCID [31]. The key difference is the addition of Secondary alignment, which extracts secondary alignment events from the modality-specific results following Primary alignment. Therefore, the ablation effects of each module are consistent. Here, we only discuss the overall ablation of the two layers of H-DCID, as detailed in rows 3 and 4 of Tab. 1. The newly added secondary alignment captures secondary alignment events, successfully aiding in the improvement of AVVP [26] and AVE2AVVP tasks, which require finer granularity. However, it also slightly impacts the primary alignment events.

Codebook Size: The impact of codebook size on performance was systematically investigated by comparing five distinct sizes in conjunction with the DCID and H-DCID modules, as depicted in Fig. 5. It was observed that the integration of the H-DCID module consistently led to a marginal decline in performance on the AVE [27] dataset, while simultaneously achieving substantial enhancements on the AVVP [26] and AVE2AVVP datasets. The TOC module demonstrated a remarkable generalization capability, contributing to performance improvements across all evaluated downstream tasks and codebook sizes. Notably, the optimal codebook size was identified to be 400, with the average performance exhibiting an initial increase followed by a subsequent decrease as the codebook size

expanded. This result underscores the importance of selecting an appropriate codebook size to achieve optimal performance in multimodal learning tasks.

6 Conclusion

In this study, inspired by works related to feature importance and combined with the concept of training-free optimization, we propose the Training-Free Optimization Codebook (TOC). To the best of our knowledge, this is the first work to apply training-free optimization to the unified discrete representation space. Furthermore, we explored the potential of DCID as a multimodal unified discrete representation space and extended it to H-DCID, extracting latent secondary event information that DCID [31] could not retain, thereby enhancing the model’s performance in tasks requiring finer granularity.

Our exploration also includes replacing vector quantization with more complex or novel quantization methods. While these methods significantly improve the performance of trained modalities, they do not enhance cross-modal generalization; in some cases, they even reduce overall effectiveness. This highlights a crucial direction for future research: designing more suitable quantization methods to promote cross-modal generalization.

References

1. Andonian, A., Chen, S., Hamid, R.: Robust cross-modal representation learning with progressive self-distillation. In: *Proceedings of the IEEE/CVF Conference on Computer Vision and Pattern Recognition*. pp. 16430–16441 (2022)
2. Barnes, C., Rizvi, S., Nasrabadi, N.: Advances in residual vector quantization: a review. *IEEE Transactions on Image Processing* **5**(2), 226–262 (1996). <https://doi.org/10.1109/83.480761>
3. Breiman, L.: Random forests. *Machine learning* **45**, 5–32 (2001)
4. Chen, M., Laina, I., Vedaldi, A.: Training-free layout control with cross-attention guidance. In: *Proceedings of the IEEE/CVF Winter Conference on Applications of Computer Vision*. pp. 5343–5353 (2024)
5. Chen, Y.C., Li, L., Yu, L., El Kholy, A., Ahmed, F., Gan, Z., Cheng, Y., Liu, J.: Uniter: Universal image-text representation learning. In: *European conference on computer vision*. pp. 104–120. Springer (2020)
6. Cheng, P., Hao, W., Dai, S., Liu, J., Gan, Z., Carin, L.: Club: A contrastive log-ratio upper bound of mutual information. In: *International conference on machine learning*. pp. 1779–1788. PMLR (2020)
7. Devlin, J., Chang, M.W., Lee, K., Toutanova, K.: Bert: Pre-training of deep bidirectional transformers for language understanding. *arXiv preprint arXiv:1810.04805* (2018)
8. Duan, J., Chen, L., Tran, S., Yang, J., Xu, Y., Zeng, B., Chilimbi, T.: Multi-modal alignment using representation codebook. In: *Proceedings of the IEEE/CVF Conference on Computer Vision and Pattern Recognition*. pp. 15651–15660 (2022)
9. Duke, B., Ahmed, A., Wolf, C., Aarabi, P., Taylor, G.W.: Sstvos: Sparse spatiotemporal transformers for video object segmentation. In: *Proceedings of the IEEE/CVF Conference on Computer Vision and Pattern Recognition*. pp. 5912–5921 (2021)
10. Harwath, D., Recasens, A., Surís, D., Chuang, G., Torralba, A., Glass, J.: Jointly discovering visual objects and spoken words from raw sensory input. In: *Proceedings of the European conference on computer vision (ECCV)*. pp. 649–665 (2018)
11. Liu, A.H., Jin, S., Lai, C.I.J., Rouditchenko, A., Oliva, A., Glass, J.: Cross-modal discrete representation learning. *arXiv preprint arXiv:2106.05438* (2021)
12. Liu, X., Gong, C., Wu, L., Zhang, S., Su, H., Liu, Q.: Fusedream: Training-free text-to-image generation with improved clip+ gan space optimization. *arXiv preprint arXiv:2112.01573* (2021)
13. Lu, J., Clark, C., Zellers, R., Mottaghi, R., Kembhavi, A.: Unified-io: A unified model for vision, language, and multi-modal tasks. *arXiv preprint arXiv:2206.08916* (2022)
14. Luo, H., Ji, L., Zhong, M., Chen, Y., Lei, W., Duan, N., Li, T.: Clip4clip: An empirical study of clip for end to end video clip retrieval and captioning. *Neuro-computing* **508**, 293–304 (2022)
15. Mentzer, F., Minnen, D., Agustsson, E., Tschannen, M.: Finite scalar quantization: Vq-vae made simple. *arXiv preprint arXiv:2309.15505* (2023)
16. Miech, A., Zhukov, D., Alayrac, J.B., Tapaswi, M., Laptev, I., Sivic, J.: Howto100m: Learning a text-video embedding by watching hundred million narrated video clips. In: *Proceedings of the IEEE/CVF international conference on computer vision*. pp. 2630–2640 (2019)
17. Monfort, M., Jin, S., Liu, A., Harwath, D., Feris, R., Glass, J., Oliva, A.: Spoken moments: Learning joint audio-visual representations from video descriptions.

- In: Proceedings of the IEEE/CVF Conference on Computer Vision and Pattern Recognition. pp. 14871–14881 (2021)
18. Oord, A.v.d., Li, Y., Vinyals, O.: Representation learning with contrastive predictive coding. arXiv preprint arXiv:1807.03748 (2018)
 19. Pedersoli, F., Wiebe, D., Banitalebi, A., Zhang, Y., Tzanetakis, G., Yi, K.M.: Estimating visual information from audio through manifold learning. arXiv preprint arXiv:2208.02337 (2022)
 20. Petridis, S., Stafylakis, T., Ma, P., Tzimiropoulos, G., Pantic, M.: Audio-visual speech recognition with a hybrid ctc/attention architecture. In: 2018 IEEE Spoken Language Technology Workshop (SLT). pp. 513–520. IEEE (2018)
 21. Radford, A., Kim, J.W., Hallacy, C., Ramesh, A., Goh, G., Agarwal, S., Sastry, G., Askell, A., Mishkin, P., Clark, J., et al.: Learning transferable visual models from natural language supervision. In: International conference on machine learning. pp. 8748–8763. PMLR (2021)
 22. Sarkar, P., Etemad, A.: Xkd: Cross-modal knowledge distillation with domain alignment for video representation learning. arXiv preprint arXiv:2211.13929 (2022)
 23. Shvetsova, N., Chen, B., Rouditchenko, A., Thomas, S., Kingsbury, B., Feris, R.S., Harwath, D., Glass, J., Kuehne, H.: Everything at once-multi-modal fusion transformer for video retrieval. In: Proceedings of the IEEE/CVF conference on computer vision and pattern recognition. pp. 20020–20029 (2022)
 24. Simonyan, K., Zisserman, A.: Very deep convolutional networks for large-scale image recognition. arXiv preprint arXiv:1409.1556 (2014)
 25. Soomro, K., Zamir, A.R., Shah, M.: Ucf101: A dataset of 101 human actions classes from videos in the wild. arXiv preprint arXiv:1212.0402 (2012)
 26. Tian, Y., Li, D., Xu, C.: Unified multisensory perception: Weakly-supervised audio-visual video parsing. In: Computer Vision–ECCV 2020: 16th European Conference, Glasgow, UK, August 23–28, 2020, Proceedings, Part III 16. pp. 436–454. Springer (2020)
 27. Tian, Y., Shi, J., Li, B., Duan, Z., Xu, C.: Audio-visual event localization in unconstrained videos. In: Proceedings of the European Conference on Computer Vision (ECCV). pp. 247–263 (2018)
 28. Wang, Q.W., Zhou, D.W., Zhang, Y.K., Zhan, D.C., Ye, H.J.: Few-shot class-incremental learning via training-free prototype calibration. *Advances in Neural Information Processing Systems* **36** (2024)
 29. Wang, T., Jiang, W., Lu, Z., Zheng, F., Cheng, R., Yin, C., Luo, P.: Vlmixer: Unpaired vision-language pre-training via cross-modal cutmix. In: International Conference on Machine Learning. pp. 22680–22690. PMLR (2022)
 30. Wojtas, M., Chen, K.: Feature importance ranking for deep learning. *Advances in Neural Information Processing Systems* **33**, 5105–5114 (2020)
 31. Xia, Y., Huang, H., Zhu, J., Zhao, Z.: Achieving cross modal generalization with multimodal unified representation. *Advances in Neural Information Processing Systems* **36** (2024)
 32. Xu, H., Ghosh, G., Huang, P.Y., Okhonko, D., Aghajanyan, A., Metze, F., Zettlemoyer, L., Feichtenhofer, C.: Videoclip: Contrastive pre-training for zero-shot video-text understanding. arXiv preprint arXiv:2109.14084 (2021)
 33. Xue, Z., Gao, Z., Ren, S., Zhao, H.: The modality focusing hypothesis: Towards understanding crossmodal knowledge distillation. arXiv preprint arXiv:2206.06487 (2022)

34. You, H., Zhou, L., Xiao, B., Codella, N., Cheng, Y., Xu, R., Chang, S.F., Yuan, L.: Learning visual representation from modality-shared contrastive language-image pre-training. In: *Computer Vision–ECCV 2022: 17th European Conference, Tel Aviv, Israel, October 23–27, 2022, Proceedings, Part XXVII*. pp. 69–87. Springer (2022)
35. Zhang, R., Zhang, W., Fang, R., Gao, P., Li, K., Dai, J., Qiao, Y., Li, H.: Tip-adapter: Training-free adaption of clip for few-shot classification. In: *European Conference on Computer Vision*. pp. 493–510. Springer (2022)
36. Zhao, Y., Zhang, C., Huang, H., Li, H., Zhao, Z.: Towards effective multi-modal interchanges in zero-resource sounding object localization. *Advances in Neural Information Processing Systems* **35**, 38089–38102 (2022)
37. Zhou, J., Guo, D., Wang, M.: Contrastive positive sample propagation along the audio-visual event line. *IEEE Transactions on Pattern Analysis and Machine Intelligence* (2022)
38. Zhou, J., Wang, J., Zhang, J., Sun, W., Zhang, J., Birchfield, S., Guo, D., Kong, L., Wang, M., Zhong, Y.: Audio-visual segmentation. In: *Computer Vision–ECCV 2022: 17th European Conference, Tel Aviv, Israel, October 23–27, 2022, Proceedings, Part XXXVII*. pp. 386–403. Springer (2022)
39. Zhou, J., Zheng, L., Zhong, Y., Hao, S., Wang, M.: Positive sample propagation along the audio-visual event line. In: *Proceedings of the IEEE/CVF Conference on Computer Vision and Pattern Recognition*. pp. 8436–8444 (2021)
40. Zhu, X., Zhang, R., He, B., Zhou, A., Wang, D., Zhao, B., Gao, P.: Not all features matter: Enhancing few-shot clip with adaptive prior refinement. *arXiv preprint arXiv:2304.01195* (2023)

Appendix

A Detailed derivations or explanations for all formulas and losses about H-DCID

The architecture of H-DCID fundamentally mirrors that of DCID [31], yet it incorporates additional modules to capture latent secondary events across modalities, in contrast to DCID which aligns only the primary common events among modalities. The main components consist of two aspects: MI minimization between modality-general information and modality-specific information within each modality using CLUB [6], and MI maximization between modality-general information across different modalities using Cross-Modal CPC [18].

Given three paired modalities, $(\mathbf{x}_i^a, \mathbf{x}_i^b, \mathbf{x}_i^c)_{i=1}^N$, we employ three modality-specific encoders Ψ^a, Ψ^b, Ψ^c to extract modality-specific features $\bar{\mathbf{z}}_i^a, \bar{\mathbf{z}}_i^b, \bar{\mathbf{z}}_i^c$, and three modality-general encoders Φ^a, Φ^b, Φ^c to extract modality-general features $\mathbf{z}_i^a, \mathbf{z}_i^b, \mathbf{z}_i^c \in \mathbb{R}^{T \times D}$ from modalities A, B, and C, respectively. Compared to DCID, which requires only one set of the aforementioned encoders, H-DCID necessitates 2 sets:

$$\mathbf{z}_{i,k}^m = \Phi_k^m(\mathbf{x}_{i,k}^m), \bar{\mathbf{z}}_{i,k}^m = \Psi_k^m(\mathbf{x}_{i,k}^m), m \in \{a, b, c\}, k \in \{1, 2\}. \quad (1)$$

Furthermore, the input to all second-layer encoders is the output of the first-layer modality-general result:

$$\mathbf{x}_{i,2}^m = \bar{\mathbf{z}}_{i,1}^m. \quad (2)$$

The latent codebook $\mathbf{e} \in \mathbb{R}^{L \times D \times K}$ is shared across modalities A, B, and C, where T, L, D, and K represent time, size of the discrete latent space, hidden dimension, and layer num of codebook, respectively. The dimension of $\bar{\mathbf{z}}_{i,k}^a, \bar{\mathbf{z}}_{i,k}^b, \bar{\mathbf{z}}_{i,k}^c$ varies for different modalities. Apply vector quantized operation to map model-general feature $\mathbf{z}_{i,k}^a, \mathbf{z}_{i,k}^b, \mathbf{z}_{i,k}^c$ to discrete latent codes, $t \in [0, T)$:

$$\begin{aligned} \hat{\mathbf{z}}_{i,k,t}^m &= VQ(\Phi_k^m(\mathbf{x}_{i,k}^m)) = VQ(\mathbf{z}_{i,k,t}^m) = e_{l,k}, \\ \text{where } l &= \underset{j}{\operatorname{argmin}} \|\Phi_k^m(x) - e_{j,k}\|_2, m \in \{a, b, c\}, k \in \{1, 2\}. \end{aligned} \quad (3)$$

Then, we combine $\hat{\mathbf{z}}_{i,k}^m$ with $\bar{\mathbf{z}}_{i,k}^m$ together to reconstruct original features:

$$\sum_{k=1}^K \left(\underbrace{\|\mathbf{x}_{i,k}^m - D(\hat{\mathbf{z}}_{i,k}^m; \bar{\mathbf{z}}_{i,k}^m)\|_2^2}_{\text{reconstruction loss}} + \underbrace{\|\operatorname{sg}[\phi_k^m(\mathbf{x}_{i,k}^m)] - \mathbf{e}\|_2^2}_{\text{VQ loss}} + \underbrace{\beta \|\phi_k^m(\mathbf{x}_{i,k}^m) - \operatorname{sg}[\mathbf{e}]\|_2^2}_{\text{commitment loss}} \right), \quad (4)$$

$m \in \{a, b, c\}, k \in \{1, 2\},$

where β is set to 0.25, and sg denotes the stop gradient operation. We employ the Exponential Moving Average (EMA) strategy to replace the Vector Quantization (VQ) loss, and utilize the Multi-modal Exponential Moving Average

(MM-EMA) [31] to modify the commitment loss. The reconstruction loss ensures that the compressed latent codes e_l retain the general information of different modalities. Ideally, $\mathbf{z}_{i,k}^a$, $\mathbf{z}_{i,k}^b$, and $\mathbf{z}_{i,k}^c$, encoded from different modalities with the same semantics, should be mapped to the same discrete latent code. However, in the absence of effective supervision, the presence of a modality gap may lead to $\mathbf{z}_{i,k}^a$, $\mathbf{z}_{i,k}^b$, and $\mathbf{z}_{i,k}^c$ converging to distinct regions of the codebook [11, 36]. Consequently, we need to minimize the mutual information between the general result and the specific result, as well as maximize the mutual information among the general results of different modalities.

Mutual Information Minimization: CLUB [6] could optimize the mutual information upper bound, demonstrating superior advantages in information disentanglement. Given two variables \mathbf{x} and \mathbf{y} , the objective function of CLUB is defined as:

$$I_{vCLUB}(\mathbf{x}; \mathbf{y}) := \mathbb{E}_{p(\mathbf{x}, \mathbf{y})}[\log q_\theta(\mathbf{y}|\mathbf{x})] - \mathbb{E}_{p(\mathbf{x})}\mathbb{E}_{p(\mathbf{y})}[\log q_\theta(\mathbf{y}|\mathbf{x})]. \quad (5)$$

We use CLUB to optimize the MI upper bound between the modal-general features $\mathbf{z}_{i,k}^m$ and modal-specific features $\bar{\mathbf{z}}_{i,k}^m$, q_θ , $m \in \{a, b, c\}$, where q_θ is the variational approximation of ground-truth posterior of \mathbf{y} given \mathbf{x} and can be parameterized by a network θ .

$$\begin{aligned} \hat{I}_{vCLUB} &= \frac{1}{N} \frac{1}{K} \sum_{i=1}^N \sum_{k=1}^K \left[\frac{1}{T} \sum_{t=1}^T \log q_\theta(\bar{\mathbf{z}}_{i,k}^m | \mathbf{z}_{i,k}^m) - \frac{1}{N} \frac{1}{T} \sum_{j=1}^N \sum_{t=1}^T \log q_\theta(\bar{\mathbf{z}}_{j,k}^m | \mathbf{z}_{i,k}^m) \right], \\ m &\in \{a, b, c\}, k \in \{1, 2\}. \end{aligned} \quad (6)$$

Mutual Information Maximization: Contrastive Predictive Coding (CPC) [18] aims to maximize the mutual information between sequence items by predicting future samples using autoregressive models and is widely adopted in self-supervised learning. Humans possess the ability to not only predict subsequent scenarios from a current modality but also to associate potential situations in other modalities, such as inferring forthcoming audio from video or text or envisioning subsequent scenes from audio. Inspired by this cross-modal inference capability, Xia *et al.* [31] extend CPC to cross-modal contrastive predictive coding. Given the general features $\mathbf{z}^a, \mathbf{z}^b, \mathbf{z}^c \in \mathbb{R}^{T \times D}$, a prediction horizon of R steps, and a random time moment $t \in (0, T-R]$, two single-layer unidirectional LSTMs are used to summarize the information of all $\mathbf{z}_{\leq t}^a, \mathbf{z}_{\leq t}^b, \mathbf{z}_{\leq t}^c$, yielding three context representations as $\mathbf{c}_t^m = \text{LSTM}(\mathbf{z}_{\leq t}^m \in \mathbb{R}^D, m \in a, b, c)$.

For modality M , we first select a set Z^n of $N-1$ random negative samples and one positive sample \mathbf{z}_{t+r}^n from modality N , then use \mathbf{c}_t^m to predict r -th future step \mathbf{z}_{t+r}^n in modality N , and the InfoNCE loss for all modality can be optimized as:

$$L_{cpc}^{m2n} = -\frac{1}{R} \frac{1}{K} \sum_{r=1}^R \sum_{k=1}^K \log \left[\frac{\exp(\mathbf{z}_{t+r,k}^n W_{r,k}^m \mathbf{c}_{t,k}^m)}{\sum_{\mathbf{z}_j \in Z_n} \exp(\mathbf{z}_{j,k}^n W_{r,k}^m \mathbf{c}_{t,k}^m)} \right], \quad m, n \in \{a, b, c\}, \quad k \in \{1, 2\}. \quad (7)$$

The overall objective of H-DCID is a combination of these loss functions across both layers:

$$L = L_{\text{recon}} + L_{\text{commit}} + L_{\text{cpc}} + L_{\text{cmcm}} + L_{\text{MI}}, \quad (8)$$

where L_{recon} is the reconstruction loss that merges the modality-specific and modality-general results for each modality and compares them with the original input using MSE loss, L_{commit} is the commitment loss that computes the MSE loss between the modality-general results and their quantized codes, L_{cpc} is the Contrastive Predictive Coding loss that enhances cross-modal alignment and inference by predicting future samples in one modality using information from another, L_{cmcm} is the objective loss proposed in [11], which also promotes the alignment among modalities, and L_{MI} represents the mutual information loss concerning the modality-specific and modality-general results within each modality.

Differences between H-DCID and DCID: The primary distinction between H-DCID and DCID lies in the second layer of H-DCID, which aims to capture secondary events for a more nuanced understanding of cross-modal relationships. This hierarchical approach enables H-DCID to provide a more comprehensive representation of multimodal data, enhancing its performance in downstream tasks that require fine-grained semantic understanding.